Published in final edited form as:
Nano Lett. 2008 December ; 8(12): 4108–4115. doi:10.1021/nl8019888.

Encapsulation of Organic Molecules in Calcium Phosphate Nanocomposite Particles for Intracellular Imaging and Drug Delivery

Thomas T. Morgan[†], **Hari S. Muddana**[‡], **Erhan I. Altinoğlu**[†], **Sarah M. Rouse**[†], **Amra Tabaković**[†], **Tristan Tabouillot**[‡], **Timothy J. Russin**[§], **Sriram S. Shanmugavelandy**[⊥], **Peter J. Butler**[‡], **Peter C. Eklund**[§], **Jong K. Yun**[⊥], **Mark Kester**[⊥], and **James H. Adair**[†,*]

[†]Material Science and Engineering Department, The Pennsylvania State University, 249 Materials Research Laboratories, Hastings Road, University Park, Pennsylvania 16802

[‡]Department of Bioengineering, The Pennsylvania State University, 205 Hallowell Building, University Park, Pennsylvania 16802

[§]Departments of Physics and Materials Science and Engineering, The Pennsylvania State University, 104 Davey Laboratory, University Park, Pennsylvania 16802

[⊥]Department of Pharmacology, Penn State Milton S. Hershey Medical Center,. Hershey, Pennsylvania 17033

Abstract

Encapsulation of imaging agents and drugs in calcium phosphate nanoparticles (CPNPs) has potential as a nontoxic, bioresorbable vehicle for drug delivery to cells and tumors. The objectives of this study were to develop a calcium phosphate nanoparticle encapsulation system for organic dyes and therapeutic drugs so that advanced fluoresence methods could be used to assess the efficiency of drug delivery and possible mechanisms of nanoparticle bioabsorption. Highly concentrated CPNPs encapsulating a variety of organic fluorophores were successfully synthesized. Well-dispersed CPNPs encapsulating Cy3 amidite exhibited nearly a 5-fold increase in fluorescence quantum yield when compared to the free dye in PBS. FCS diffusion data and cell staining were used to show pH-dependent dissolution of the particles and cellular uptake, respectively. Furthermore, an experimental hydrophobic cell growth inhibitor, ceramide, was successfully delivered *in vitro* to human vascular smooth muscle cells via encapsulation in CPNPs. These studies demonstrate that CPNPs are effective carriers of dyes and drugs for bioimaging and, potentially, for therapeutic intervention.

Encasement of fluorescent dyes and other organic molecules in nanoparticulate systems is of significant importance in the fields of drug delivery and biological imaging.[1–7] Approaches to capture organic molecules in nanoparticles is an area of intense research addressing many schemes ranging from polymeric systems[8,9] and liposomes[10] to inorganic oxides.[2,4,5,7,11–13] However, many of these systems have significant shortcomings that limit their usefulness as bioimaging agents or as drug delivery vehicles. For example, it has been shown in polymeric nanoparticles for cellular uptake that endocytosis may be immediately followed by exocytosis once the concentration gradient of particles outside the cell is removed.[8]

[*]Author for correspondence. JHA3@ems.psu.edu.

Supporting Information Available: Diffusion coefficients and hydrodynamic radii in DPBS, chemical structures, cell culture protocols, MTS assay protocol, particle size histogram. This material is available free of charge via the Internet at http://pubs.acs.org.

Exocytosis may, presumably, result from insoluble solid and amorphous nanoparticle systems and will limit their utility as drug delivery agents.[9,14] Additionally, many of the systems are difficult and time-consuming to synthesize.[15–17] This is particularly true for metallic and semiconductor nanoparticles, which often require post-preparative ligand exchanges for functionality,[15,16] and for dendrimers, which can take many hours or even days to prepare.[17] Nanometer size particles, in particular, are often difficult to disperse, especially at high ionic strength and in the presence of proteins encountered in physiological fluids, such as in the blood stream.[18]

Several inherent properties of calcium phosphate (CP) underscore the potential of this system for organic encasement with respect to drug delivery and bioimaging. CP is found throughout the body in the form of amorphous calcium phosphate (ACP) as well as crystalline hydroxyapatite (HAP), the major component of bone and tooth enamel. Additionally, both Ca^{2+} and PO_4^{3-} are found in relatively high concentrations at typically 1–5 mM in the blood-stream.[19–22] This natural occurrence of CP is one of the primary advantages over other synthetic drug delivery systems. As a biomineral, CP safely biodistributes, with dissolved material regulated via the kidneys. CP is relatively insoluble at physiological pH but has increasing solubility in the acidic environments that can occur in the body,[23] such as in endolysosomes[8,24] or around solid tumors.[25] This pH-dependent solubility provides an advantage in the delivery of multifunctional drugs, fluorescent dyes, or other organic cargo to a cell or organelle. Fluorescent dyes can be used as a tracking device for the state of the particle and give an observable indication of cargo delivery, while the CP matrix can serve to protect the cargo *in vivo* until it has reached the destination.

Because the formation of CP is a relatively straightforward precipitation reaction, encasement of the cargo molecules requires only that the molecule of interest be present during the particle formation. Additionally, CP is an easily substituted matrix and often forms amorphous particles under typical reaction conditions.[18,23] This property permits the inclusion of a broad variety of substitutions such as organic fluorophores or other low-molecular weight molecules.

A wide variety of calcium phosphate precipitation schemes exist,[5,7,26–28] varying from a controlled addition of a phosphate solution to a calcium solution[7] to the use of double microemulsions as templates for particle size.[5,27,28] However, an organic-capture based approach is not widely utilized.[5,7] Furthermore, none of these schemes produces colloidally stable particles with diameters under 100 nm, and significant agglomeration is usually encountered.[5,7]

A critical issue seldom reported in detail is the laundering technique(s) used to remove residual precursor contaminants. This report documents the first demonstration of the preparation of well-dispersed, organically doped, nanoscale calcium phosphate particles. Maintaining well-dispersed nanoparticles is a challenge that limits many colloidal systems.[18] Despite the importance of maintaining dispersion, many existing postsynthesis laundering schemes produce agglomerates.[5,29] Dialysis has been used to remove spectator species from calcium phosphate particle suspensions. This approach, however, leads to substantial particle agglomeration.[5] Wang et al. investigated several other laundering schemes for silica nanocomposite colloids, which included centrifugation, filtration, Soxhlet extraction, and van der Waals chromatography (via high performance liquid chromatography [HPLC]).[29] Only the van der Waals chromatography (vdW-HPLC laundering) produced stable, nonagglomerated, concentrated particles.

We have developed a general method for encapsulating small organic molecules in well-dispersed calcium phosphate nanoparticles that utilizes the vdW-HPLC scheme[29] in

modified form to launder the particles while maintaining dispersion. Herein we report the capture of a range of organic dyes (Cascade Blue, 10-(3-sulfopropyl)acridinium betaine or SAB, fluorescein sodium salt, rhodamine WT, and Cy3 amidite), as a general proof of concept study for small-molecule encasement. Figure 1 displays fluorescence from particles that have successfully encapsulated these dyes using this method and that demonstrate the ability to encapsulate a wide variety of small molecules. These dyes encompass a range of solubility in water, from very soluble (>40 mg/mL for fluorescein sodium salt) to relatively insoluble (<0.05 mg/mL for Cy3 amidite), and include a variety of functional groups (see Supporting Information). We show enhanced fluorescence emission for use in cellular imaging as well as dissolution of the particles at low pH. We utilize these properties for simultaneous fluorescence imaging of and drug delivery to vascular smooth muscle cells.

The general synthesis scheme of organically doped, functionalized calcium phosphate nanoparticles (CP-NPs) was adapted from recently published silica syntheses.[29,30] For the CPNP synthesis, two separate microemulsions (1 and 2) are formed with a cyclohexane/Igepal CO-520/water system. The molar ratio of water to surfactant is 4. Typically, 650 μL of 1×10^{-2} M $CaCl_2$ in CO_2-free deionized water is added to 14 mL of a 29 vol % solution of Igepal CO-520 in cyclohexane to form Microemulsion 1. Similarly, 650 μL of 6×10^{-3} M disodium phosphate with 8×10^{-4} M disodium silicate in CO_2-free dionized water (pH 7.4) is added to 14 mL of a 29 vol % solution of Igepal CO-520 in cyclohexane to form Microemulsion 2. Disodium silicate is present to act as a nucleation agent for the calcium phosphate.[31] The addition of the aqueous solution to the cyclo-hexane/Igepal CO-520 solution forms a self-assembled, reverse micelle suspension. The dopant is added to one of the microemulsions based on electrostatic and stability constant considerations. For instance, negatively charged molecules, such as fluorescein and Cy3 amidite, are added to Microemulsion 2 (with the phosphate solution). This procedure is used to prevent particle nucleation and growth inhibition that can occur due to calcium binding with the carboxylate- or sulfonate-groups present on many fluorophores. Water-soluble organic dyes (such as fluorescein sodium salt and rhodamine WT) are mixed with the aqueous solution before addition into the micelle. Dyes that are insoluble in water can be added in an ethanol or ethanol-water solution after the microemulsion is formed. This report will mainly focus on details of Cy3 amidite-doped CP, where 1 mL of 1×10^{-3} M Cy3 in neat ethanol is added to Microemulsion 2. The individual microemulsions are allowed to equilibrate for 3 min before 1 and 2 are mixed to form Microemulsion 3. Microemulsion 3 is allowed to undergo micellar exchange for 2 min, during which time doped CP nanoparticles precipitate in the micelles. A dispersant is then added to Microemulsion 3. For carboxy-functionalized particles, 225 μL of 1×10^{-3} M sodium citrate is added and allowed to react for 10 min. For amine-functionalized particles, 125 μL of 4×10^{-2} M aminopropyltriethoxysilane (APTES) solution in a 95:5:1 ethanol–water–acetic acid mixture is added and allowed to react for 24 h. After adding the dispersant, the reverse micelles are dissolved with 50 mL of pH-adjusted ethanol (pH 7) before laundering via the vdW-HPLC.

The difference between the relatively strong long-range van der Waals attraction associated with condensed matter (i.e., two solid particles interacting with one another) as opposed to the short-range, and weaker, van der Waals interaction between uncharged molecules and solid surfaces[22] is the basis for the vdW-HPLC approach to nanoparticle laundering. Control over the electrostatic surface charges with the mobile phase solvent provides the ability to either inhibit or promote surface charging with relatively nonpolar and polar solvents, respectively. Inhibiting the surface charging with nonpolar solvents, such as neat ethanol, permits the van der Waals attractive forces to dominate, and reversible particle deposition onto the stationary phase is achieved. By maintaining this nonpolar environment, the weakly attracted organic molecules, such as amphiphiles and free dye, can be flushed through the column while the particles remain adhered. Shifting to a more polar solvent, in this case

70:30 ethanol–water by volume, increases the surface charging on both the stationary phase as well as the nanocolloids and provides significant electrosteric repulsion to overcome the van der Waals attractive forces, allowing the particles to break off of the column and be eluted. The end result is a concentrated solution of well-dispersed nanocolloids.

Specifically, for the CPNP system the vdW-HPLC procedure is as follows: the unwashed, as-prepared nanoparticle suspension is loaded onto an appropriately functionalized column after the micelles have been dissolved with ethanol; the free organic is laundered using ethanol as the eluent; finally, the particles are eluted using 70:30 ethanol–water by volume. To launder the particles without inducing aggregation, the stationary phase must be functionalized such that the particles will associate with, but not irreversibly aggregate to, the media. In the case of the amine-terminated particles, the stationary phase consists of 1 w/o APTES-treated 20 μm silica spheres with 6.5 nm pores. Alternately, citrate-functionalized particles are washed on the as-received, negatively charged silica microspheres.

The sample, which is approximately 25 vol % cyclohexane in ethanol after micellar dissolution, is loaded onto the silica HPLC column. The CPNP colloids adhere to the silica media because negligible surface charge is present in the low dielectric media. Thus, the relatively large van der Waals attraction of the particles to the silica media in the HPLC column leads to adhesion of the nanoparticles. Subsequent washing with neat ethanol reduces the surfactant concentration from 0.2 M Igepal CO-520 to below 1×10^{-3} M after a single pass through the column. Virtually all of the free organic dye and the cyclohexane are removed and are below the limits of detection via fluorescence correlation spectroscopy (FCS) and GC–MS, respectively. This leaves the now laundered CPNP colloids adhered to the column.

During the washing step, the dye content is monitored at the characteristic absorption wavelength (for Cy3 this is 532 nm). The ethanol washing continues until the detector reaches baseline indicating removal of the unencapsulated dye. The particles, which remain on the column due to van der Waals attraction, are then eluted with a 70:30 ethanol–water solution with 5×10^{-4} M NaCl (prepared with CO_2-free deionized water, pH 7) which provides enough charge for electrostatic repulsion to dominate the nanocolloid–silica media interaction energies. The first major peak is collected. The precursor and HLPC solutions are prepared with CO_2-free deionized water to avoid carbonate contamination in the CPNPs. All solution pH measurements are performed using a Sentron ISFET pH probe calibrated against aqueous standards.

Polyethylene glycol (PEG) was conjugated to citrate-terminated CPNPs as an example of secondary functionalization through amide formation on the surface of the particle. This conjugation is performed as follows: 0.5 mg of ethyl-3-(3-dimethylaminopropyl) carbodiimide (EDCI) and 1 mg of methoxyPEG-amine (mPEG-amine, 20 kDa) in water are added to 1 mL of laundered citrate-functionalized CP nanoparticle suspension.[32] The particles are reacted for 18 h at 40 °C under continuous stirring to form amide linkages between the particles and the mPEG-amine. The PEGylated particles are then dialyzed to remove the excess EDCI and unreacted methoxyPEG-amine. The dialyzed particles remain well dispersed, and agglomeration is not induced at this step. Recent work using these PEG functionalized CPNPs has shown particle accumulation in tumor xenografts in a nude mouse model.[33]

Transmission electron microscopy (TEM) images were taken on a Phillips 420 at 120 keV, and the particles were dropped onto a carbon film grid with a copper backing. In preliminary studies, particle damage due to high electron voltage and current densities was observed. To avoid this damage to the particles from the electron beam, current densities were kept below

70 pA/cm^2. The particles are well dispersed and show no agglomeration even after drying on the TEM grid (Figure 2, see Supporting Information for distribution data). Typical particles are shown in the inset of Figure 2. The particles have a log-normal mean of 26 nm (σ_z = 8 nm, n = 124 particles) based on diameter measurements using TEM photomicrographs. Atomic force microscopy analysis (data not shown) has been used to verify the spherical particle morphology.

The calcium and phosphate ratio was measured by ICP-MS. The molar ratio of Ca:P is 0.98:1. The ratio is low compared to the synthesis ratio (1.67:1). This is likely due to the formation of calcium–dye complexes which are excluded from the particle during the synthesis.

Fluorescence correlation spectroscopy (FCS) was used to determine the solution-phase behavior of the particles in order to better understand the particulate behavior in biologically relevant solutions and to monitor only the fluorescing species. To this end we examined the free dye and the particles in DPBS (Dulbecco's phosphate buffered saline), at pH 7 and at pH 4. Low pH conditions mimicked the acidic environment of an endolysosome in which a particle would be enveloped during endocytosis.

FCS measurements were collected for free Cy3 dye at pH 4, Cy3-doped nanoparticles at pH 4 and pH 7 in DPBS. Sample autocorrelation curves are shown in Figure 3, where a shift of the curve to the right (greater characteristic diffusion time) signifies a lower diffusion coefficient and a larger hydrodynamic radius. In this case, the diffusion time of free Cy3 dye molecules is 127 μs, and that of the nanoparticles at pH 7 is 1311 μs. The mean values and standard deviations for diffusion coefficients and hydrodynamic radii are reported in Figure 4. Nanoparticles in DPBS show a diffusion coefficient $D = 2.60 \pm 0.81 \times 10^{-7}$ cm^2/s at pH 7 and $D = 28.6 \pm 0.28 \times 10^{-7}$ cm^2/s at pH 4, while free Cy3 dye shows a value of $D = 29.0 \pm 0.18 \times 10^{-7}$ cm^2/s at pH 4. The corresponding hydrodynamic diameters and standard deviations are $D_H = 18.80 \pm 3.83$ nm for the nanoparticles at pH 7, $D_H = 0.76 \pm 0.09$ nm for the nanoparticles at pH 4, and $D_H = 0.75 \pm 0.06$ nm for the free dye at pH 4. Similar results were obtained for the nanoparticles in DI water at pH 7 and pH 4 (data not shown). In addition to the diffusion data, the particle number concentration can be determined based on the number of particles that diffuse through the observation volume. The CPNP suspension has a particle number concentration of ~6×10^{14} particles/mL, based on these determinations.

These results show that, in acidic solutions, the nanoparticles have a diffusion coefficient and hydrodynamic radius equivalent to that of free Cy3, supporting the conclusion that low solution pH induces dissolution of CP and release of the encapsulated dye.

The ζ potential distributions are collected using a Brookhaven ZetaPALS ζ potential analyzer. Figure 5 shows the effect of various surface functionalities on the surface potential. The ζ potential distributions verify a strong dependence of the charge on the surface functionality. The citrate -functionalized CPNPs exhibit a reasonably high-magnitude negative charge of −29 ± 3 mV with a half-width at 16 mV. The amine- and PEG-terminated CPNPs have a mean charge of +24 ± 6 mV with a half-width of 18 mV and 3 ± 2 mV with a half-width of 14 mV, respectively. Large standard deviations are expected from neutrally charged samples due to the inherent error associated with attempts to measure particles at zero ζ potential via electrophoretic light scattering. The main utility of amino- and carboxy-surface terminations is to use them as platforms for secondary functionalization through the use of amide linkages, as demonstrated, for example, in the case of PEG attachment. It should be noted, however, that in order to use the silane coupling agent for amino-functionality, a large excess of APTES was required. This results in the formation of

a silica shell, which in turn will affect the solubility and bioresorbability of the particle. We found that if small quantities of APTES were added, low or neutral ζ potentials are present and the samples showed significant aggregation (data not shown). Other methods of amino-functionalization will be explored in future work, such as the use of aminoethyl dihydrogen phosphate or glycine to act as calcium binding agents.

As a comparison of the free dye to the encapsulated dye, the relative fluorescence quantum efficiency (QE) was determined according to techniques in the literature.[34,35] In brief, the integrated fluorescence signals of the free Cy3 and the Cy3-doped CPNPs in PBS were compared to a known reference standard with an excitation wavelength of 532 nm, and the QE was calculated using a modified relationship from Lakowicz,[36]

$$\Phi=\Phi_R \frac{M}{M_r}\frac{n^2}{n_R^2} \quad (1)$$

where Φ and Φ_R are the QE for the sample and the reference, respectively, M and M_r are the slopes of the integrated intensity versus absorption plots (Figure 6A), and n is the refractive index of each solvent. Rhodamine 6G in ethanol was used as a reference with a quantum efficiency of 0.95.[35] The Cy3-doped CPNPs exhibited a quantum efficiency of 0.202 ± 0.007 in PBS, while the free dye efficiency was 0.045 ± 0.002 in PBS within a 95% confidence interval (Figure 6C). Our measured QE for the free Cy3 dye is comparable to literature values ranging from 0.03 to 0.05.[37] Figure 6B exemplifies this enhancement in QE by comparing the fluorescence signal of the Cy3-doped CPNPs to a solution of Cy3 free dye with the same absorption at 532 nm. There is more than a 4.5-fold increase in the maximum intensity of the CPNPs versus the free dye as well as a 9 nm red shift in the peak wavelength. This enhancement is attributed to caging effects that isolate the dye from the solvent and from specific dye–dye interactions.[38] Based on the intensity per particle and the particle number concentration from the FCS measurements, there are ~5–8 dye molecules per particle.

On the basis of the results showing pH-dependent dissolution of the CPNPs in solution, we hypothesized that CPNPs would undergo dissolution when endocytosed by cells, due to the low-pH conditions that exist in endolysosomes at late-stage endocytosis. Staining of bovine aortic cells with Cy3 free dye and Cy3-encapsulated citrate-functionalized CPNPs is shown in Figure 7A and C, respectively. The staining patterns in both these cases are identical and show specific staining of internal membranous organelles, indicating that the nanoparticles have undergone dissolution and released the dye. To confirm that the process of dissolution was mediated by endocytosis, we stained cells treated with cytochalasin-D (Figure 7B and D). Cytochalasin-D drug disrupts actin polymerization which plays multiple roles in endocytosis, including coated pit formation, vesicle transport through cytoplasm, and vesicle fusion.[39] Cytochalasin-D-treated cells stained with nanoparticles show diffuse staining of the entire cytoplasm along with some bright speckles which may arise from individual nanoparticles or nanoparticle-bearing endosomes (shown in Figure 7D). In contrast to untreated cells, no specific staining of the internal membraneous organelles was seen, suggesting that the nanoparticles were intact in cells treated with Cyto-D. To further ensure that the drug treatment did not disrupt the organelles or the staining mechanism of Cy3, we stained Cyto-D treated cells with free Cy3 dye. The organelles were intact and specifically stained (Figure 7B, arrows). Active transport of the endosomes through cytoplasm mediated by actin cytoskeleton is essential for fusion of the endosomes with lysosomes in the late-stage endocytosis and disruption of this endosome–lysosome fusion process by cytochalasin-D is thought to prevent nanoparticles from reaching the lysosomes, thus preventing dissolution.[40] Together, inhibition of organelle staining by cyto-D in

nanoparticle-treated cells along with pH-dependent dissolution of CPNPs in solution suggest that nanoparticles dissolve when the endosomes carrying them fuse with lysosomes where they experience low pH.

To further verify their potential as drug delivery vehicles, amine-terminated CPNPs encasing fluorescein sodium salt and an experimental chemotherapeutic, hexanoyl-ceramide (Cer_6), were used to determine the efficacy of the particles as simultaneous imaging and drug delivery agents. Ceramides are a class of molecules currently being explored as chemotherapeutic agents that induce a selective apoptotic response in cancer cells, while predominantly inhibiting cell growth in healthy cells.[41] Confirmation of simultaneous imaging and drug delivery using ceramide-doped calcium phosphate nanoparticles is shown in Figure 8. Human vascular smooth muscle cells were chosen to demonstrate simultaneous drug delivery and fluorescence imaging. Activated vascular smooth muscle cells lead to artherosclerosis or restenosis resulting in reduced luminal cross sections in diseased arteries. Ceramide delivered via nanoliposomes reduces cell growth in these cells.[41,42] The Cer_6–fluorescein-doped CPNPs induced up to 80% cell growth inhibition at 0.2 μM ceramide (Figure 8A), an effective dose approximately 25-fold less than if ceramide was administered in DMSO (data not shown). As a control, fluorescein-encapsulated CPNPs that did not contain bioactive ceramide labeled nearly 100% of the smooth muscle cells, retaining morphological integrity and exhibiting relatively homogeneous, bright fluorescence (Figure 8B). As a further control, amine-functionalized CPNPs, without fluoroprobe or ceramide, did not induce vascular smooth muscle cytotoxicity (MTS assay) at particle numbers approaching 10^{12} particles/mL (data not shown). Taken together, these data suggest that CPNPs can be an effective strategy to deliver hydrophobic bioactive agents, such as ceramide.

In summary, 20–30 nm diameter organically doped calcium phosphate nanoparticles were prepared using a variety of fluorescent dyes. Specifically, Cascade Blue, SAB, fluorescein sodium salt, rhodamine WT, and Cy3 amidite were successfully encapsulated displaying the ability to encapsulate several varieties of small organic molecules. Comparisons of the diameter by FCS and TEM confirm solution-phase colloidal stability of the particles, as well as their spherical morphology. Additionally, the fluorescence quantum efficiency exhibited nearly a 4-fold increase from 0.045 to 0.202 for the free and encapsulated dye, respectively. Dissolution of the particles at low pH was proven by a shift in the diffusion coefficient to larger values, indicating a release of encapsulated contents in environments similar to that of endolysosomes. As further proof of this property, bovine aortic cells were effectively stained with the particles, and dissolution was inhibited through the use of cytochalasin-D. Preliminary drug delivery results show that a hydrophobic chemotherapeutic, such as ceramide, can be delivered *in vitro* to human vascular cells. Both carboxy- and amino-functional nanoparticles were prepared, and the carboxy-terminal particles were successfully used as a platform for PEG functionalization. Current and future work is focused on the use of the CPNPs for both bioimaging and drug delivery.

Supplementary Material

Refer to Web version on PubMed Central for supplementary material.

Acknowledgments

This work was supported by Keystone Nano, Inc. and in part by grants to Peter J. Butler from the National Heart Lung and Blood Institute (R01 HL 07754201-A1) and the National Science Foundation (CAREER Award BES 0238910). TEM work was performed in the electron microscopy facility of the Materials Research Institute at The Pennsylvania State University.

References

1. Vasir JK, Labhestwar V. Adv. Drug Delivery Rev. 2007; 59:718–728.
2. Ow H, Larson DR, Srivastava M, Baird BA, Webb WW, Wiesner U. Nano Lett. 2005; 5:113–117. [PubMed: 15792423]
3. Jin S, Ye K. Biotechnol. Prog. 2007; 23:32–41. [PubMed: 17269667]
4. Xu ZP, Zeng QH, Lu GQ, Yu AB. Chem. Eng. Sci. 2006; 61:1027–1040.
5. Bisht S, Bhakta G, Mitra S, Maitra AN. Int. J. Pharm. 2004; 288:157–168. [PubMed: 15607268]
6. Yao G, Wang L, Wu Y, Smith J, Xu J, Zhao W, Lee E, Tan W. Anal. Bioanal. Chem. 2006; 385:518–524. [PubMed: 16715275]
7. Welzel T, Radtke I, Meyer-Zaika W, Heumann R, Epple M. J. Mater. Chem. 2004; 14:2213–2217.
8. Panyam J, Labhestwar V. AdV. Drug DeliVery Rev. 2003; 55:329–347.
9. Park JS, Han TH, Lee KY, Han SS, Hwang JJ, Moon DH, Kim SY, Cho YW. J. Controlled Release. 2006; 115:37–45.
10. Stover TC, Sharma A, Robertson GP, Kester M. Clin. Cancer Res. 2005; 11(9):3465–3474. [PubMed: 15867249]
11. Bagwe RP, Yang C, Hilliard LR, Tan W. Langmuir. 2005; 20:8336–8342. [PubMed: 15350111]
12. Bele M, Siiman O, Matijevic E. J. Colloid Interface Sci. 2002; 254:274–282. [PubMed: 12702398]
13. Fuller JE, Zugates GT, Ferreira LS, Ow HS, Nguyen NN, Wiesner UB, Langer RS. Biomaterials. 2008; 29:1526–1532. [PubMed: 18096220]
14. Chithrani BD, Chan WCW. Nano Lett. 2007; 7(6):1542–1550. [PubMed: 17465586]
15. Tan WB, Zhang Y. J. Biomed. Mater. Res. Part A. 2005; 75A(1):56–62.
16. Joshi HM, Bhumkar DR, Joshi K, Pokharkar V, Sastry M. Langmuir. 2006; 22(1):300–305. [PubMed: 16378435]
17. Dhanikula RS, Hildgen P. Bioconjugate Chem. 2006; 17:29–41.
18. Adair, JH.; Kumar, R.; Antolino, N.; Szepesi, CJ.; Kimel, RA.; Rouse, SM. Colloidal Lessons Learned for Dispersion of Nanosize Particulate Suspensions. In: Baumard, JF., editor. Lessons in Nanotechnology from Traditional and Advanced Ceramics, Proceedings of the FORUM 2004 of the World Academy of Ceramics; Faenza, Italy, May 2004. Faenza, Italy: Techna Group; 2005. p. 93-145.
19. Wang S, McDonnell EH, Sedor FA, Toffaletti JG. Arch. Pathol. Lab. Med. 2002; 126:947–950. [PubMed: 12171493]
20. Alberts, B.; Johnson, A.; Lewis, J.; Raff, M.; Roberts, K.; Walter, P. Molecular Biology of The Cell. 4th ed.. New York: Garland Science; 2002.
21. Coe, FL.; Favus, MJ.; Pak, CYC.; Parks, JH.; Preminger, GM. Kidney Stones: Medical and Surgical Management. Philadelphia: Lippincott-Raven; 1996.
22. Israelachvili, J. Intermolecular and Surface Forces. 2nd ed.. London: Acdemic Press; 1992.
23. Tung, MS. Calcium Phosphates: Structure, Composition, Solubility, and Stability. In: Amjad, Z., editor. Calcium Phosphates in Biological and Industrial Systems. Boston: Kluwer Academic Publishers; 1998. p. 1-19.
24. Tycko B, Maxfield FR. Cell. 1982; 26:643–651. [PubMed: 6176331]
25. Stubbs M, McSheehy PMJ, Griffiths JR, Bashford CL. Mol. Med. Today. 2000; 6:15–19. [PubMed: 10637570]
26. Tang R, Wang L, Nancollas GH. J. Mater. Chem. 2004; 14:2341–2346.
27. Sadasivan S, Khushalani D, Mann S. Chem. Mater. 2005; 17:2765–2770.
28. Sarda S, Heughebaert M, Lebugle A. Chem. Mater. 1999; 11:2722–2727.
29. Wang J, White WB, Adair JH. J. Phys. Chem. B. 2006; 110:4679–4685. [PubMed: 16526702]
30. Li T, Moon J, Morrone AA, Mecholsky JJ, Talham DR, Adair JH. Langmuir. 1999; 15:4328–4334.
31. Adair, JH.; Nagira, T.; Brown, CM.; Khan, SR.; Thomas, WCJ. Heterogeneous Deposition of Calcium Phosphates at the Silicon (Hydrous) Oxide-Water Interface. In: Ryall, R.; Bias, R.; Marshall, VR.; Rofe, AM.; Smith, LH.; Walker, VR., editors. Urolithiasis 2. New York: Plenum Press; 1995. p. 181-187.

32. Sharma RK, Das S, Maitra A. J. Colloid Interface Sci. 2004; 277:324–346.
33. Altinoğlu Eİ, Russin TJ, Kaiser JM, Barth BM, Eklund PC, Kester M, Adair JH. Near-Infrared Emitting Fluorophore-Doped Calcium Phosphate Nanoparticles for In Vivo Imaging of Human Breast Cancer. ACS Nano. 2008 Published on the Internet September 19, 2008 http://pubs.acs.org/cgibin/abstract.cgi/ancac3/asap/abs/nn800448r.html.
34. Williams ATR, Winfield SA, Miller JN. Analyst. 1983; 108:1067–1071.
35. Kubin RF, Fletcher AN. J. Lumin. 1982; 27:455–462.
36. Lakowicz, JR. Principles of Fluorescence Spectroscopy. 3rd ed.. New York: Springer Science and Business Media; 2006. p. 54
37. Southwick PL, Ernst LA, Tauriello EW, Parker SR, Mujumdar RB, Mujumdar SR, Cleaver HA, Waggoner AS. Cytometry. 1990; 11:418–430. [PubMed: 2340776]
38. Avnir D, Levy D, Reisfeld R. J. Phys. Chem. B. 1984; 88:5956–5959.
39. Qualmann B, Kessels MM, Kelly RB. J. Cell Biol. 2000; 150:F111–F116. [PubMed: 10974009]
40. Mellman I. Annu. Rev. Cell Dev. Biol. 1996; 12:575–625. [PubMed: 8970738]
41. Bourbon NA, Sandirasegarane L, Kester M. J. Biol. Chem. 2002; 277:3286–3292. [PubMed: 11723139]
42. Charles R, Sandirasegarane L, Yun J, Bourbon NA, Rothstein R, Wilson R, Levinson SW, Kester M. Circ. Res. 2000; 87(4):282–288. [PubMed: 10948061]

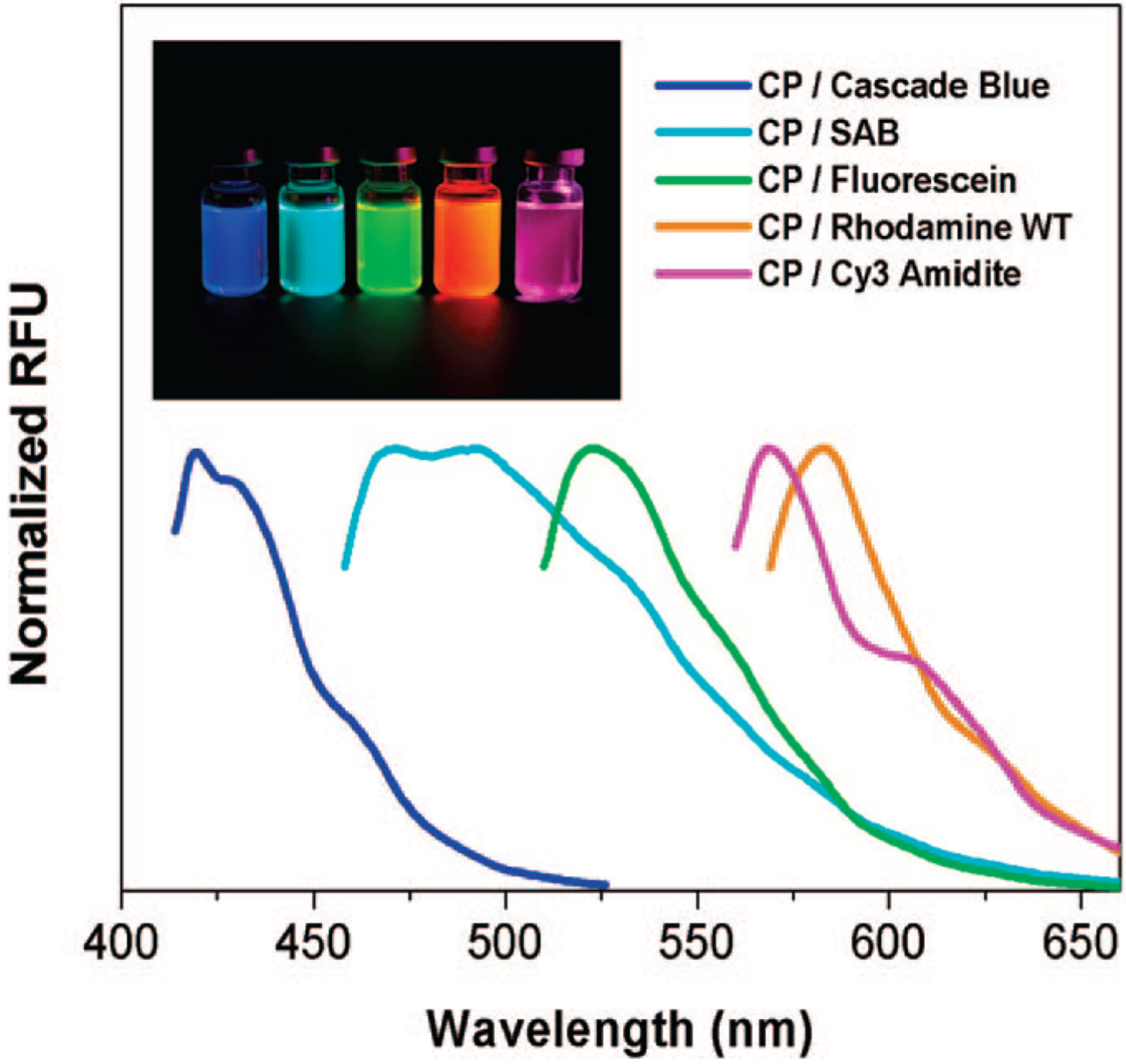

Figure 1.

Fluorescence spectra of a range of dye-encapsulated calcium phosphate nanocomposite particles show Cascade Blue (dark blue), 10-(3-sulfopropyl) acridinium betaine (SAB; light blue), fluorescein (green), rhodamine WT (orange), and Cy3 amidite (magenta) encapsulated in calcium phosphate nanoparticles. (Inset) Photograph taken under UV lamp excitation displaying the fluorescence of encapsulated fluorophores. From left to right: Cascade Blue, SAB, fluorescein, rhodamine WT, and Cy3 amidite.

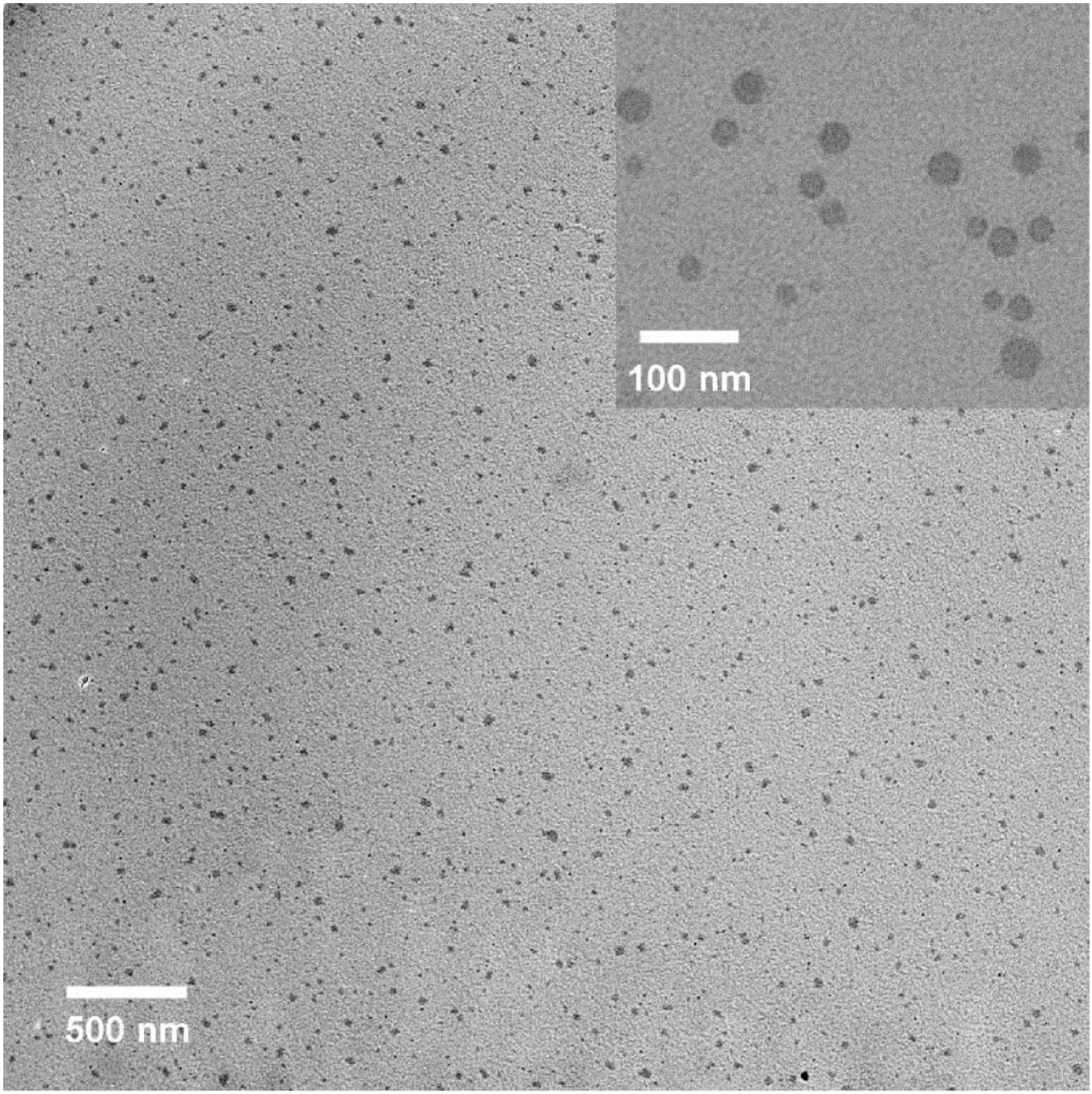

Figure 2.
TEM micrograph shows well-dispersed spherical particles on a carbon film grid. (Inset) Morphology in detail.

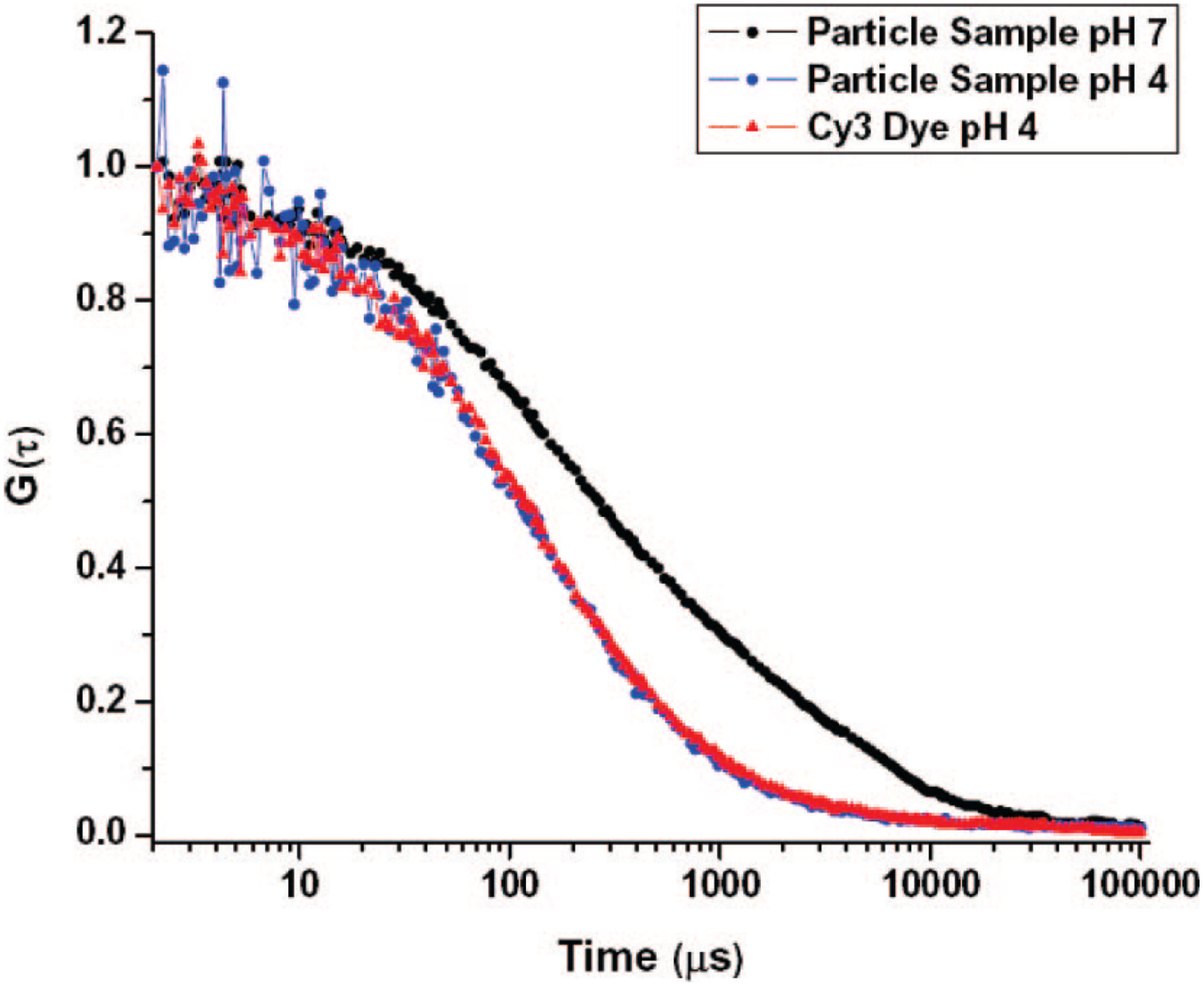

Figure 3.
Sample autocorrelation curves of nanoparticles in pH 7 (black), nanoparticles in pH 4 (blue), and free Cy3 dye in pH 4 (red).

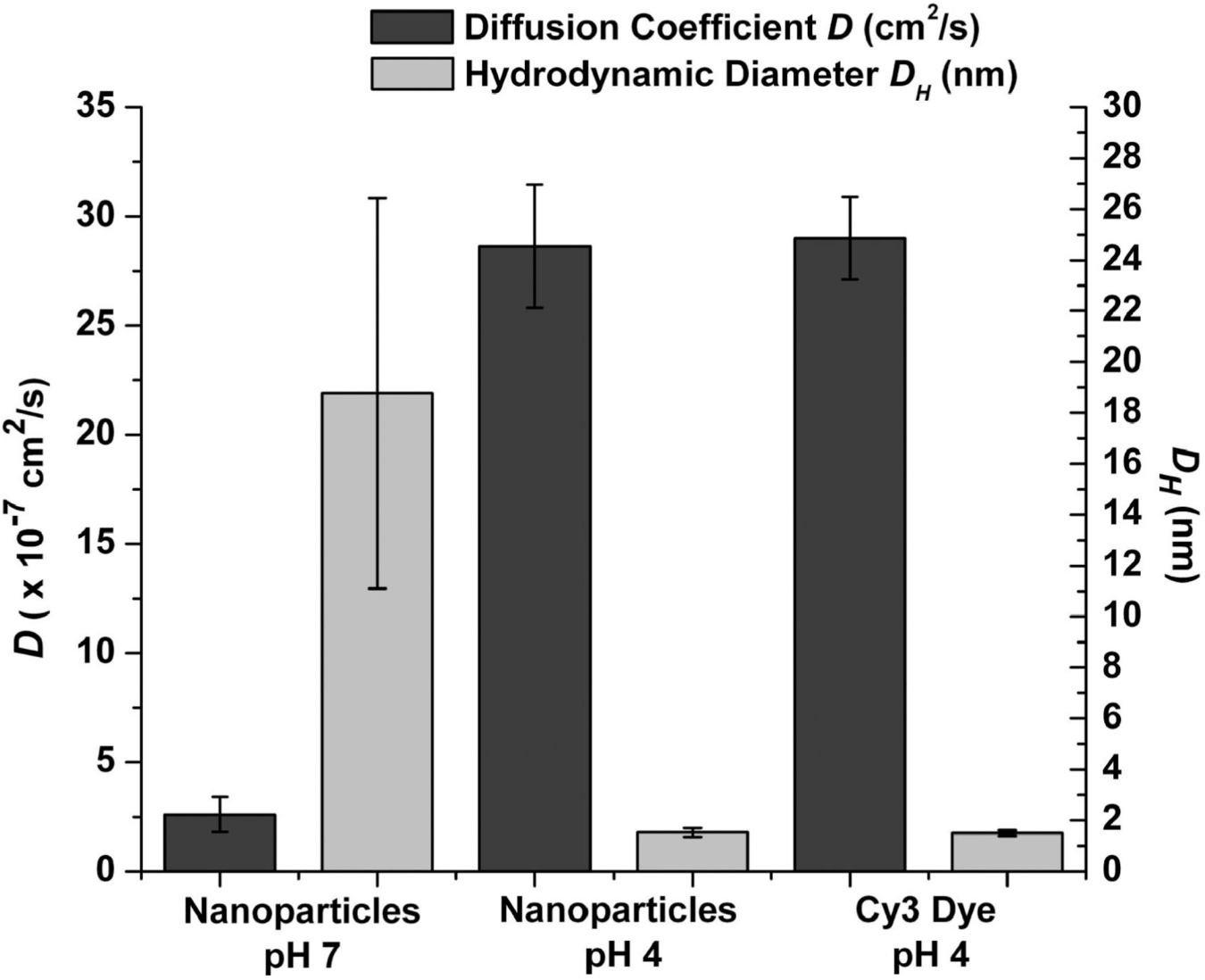

Figure 4.

Diffusion coefficient *D* (black) and hydrodynamic diameter (gray) of free Cy3 dye at pH 4 and nanoparticles at pH 4 and pH 7. **p* < 0.0001 for pH 4 vs pH 7. No significant difference for *D* (D_H) was detected between nanoparticle samples and Cy3 for pH 4. The standard deviation of the particle sample at pH 7 reflects the distribution in particle diameters.

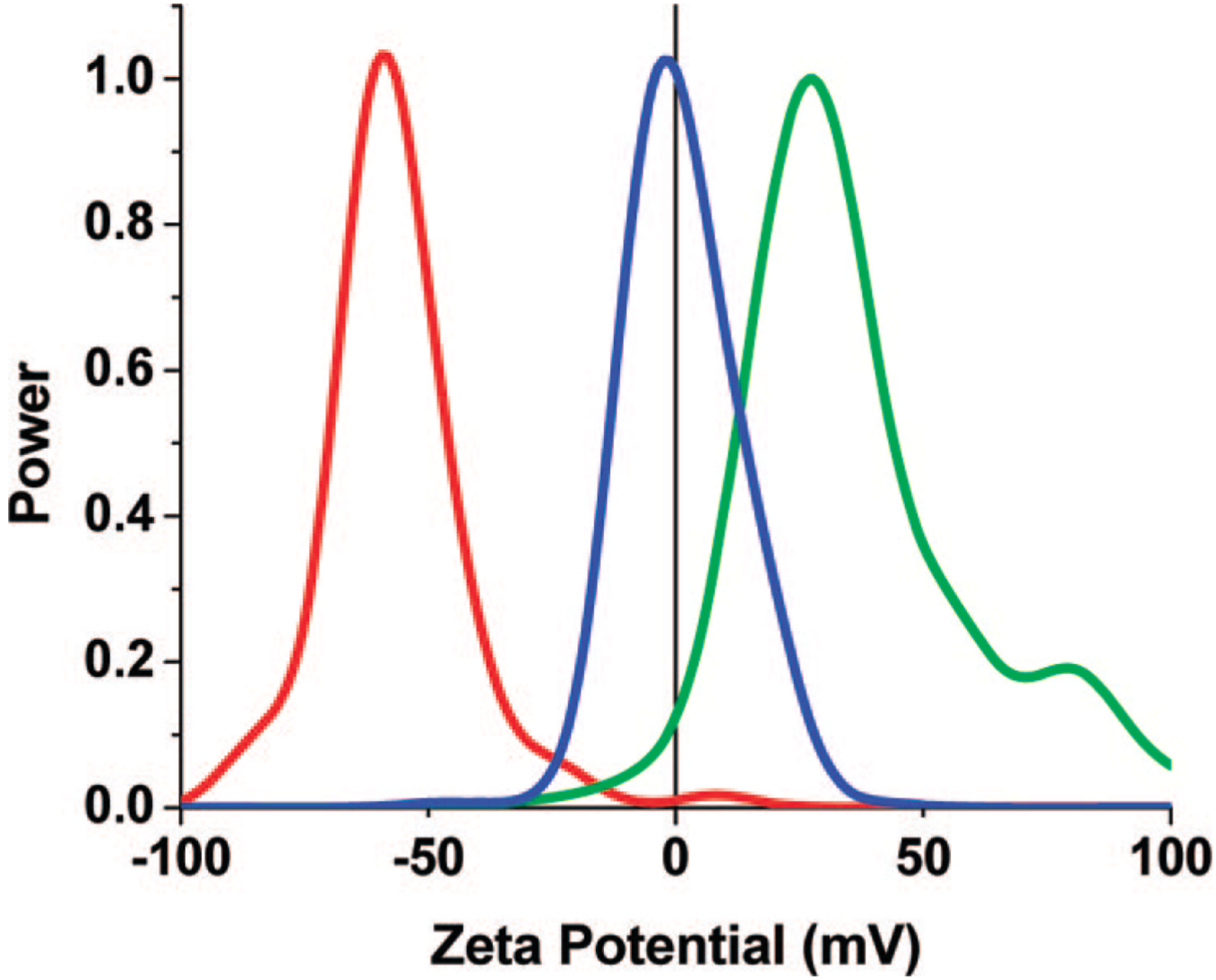

Figure 5.

ζ potential distributions of the CPNPs with various surface terminations in 70:30 EtOH–H_2O at pH 6–7. The COO^--terminated particles (red line) have a mean ζ potential of −30 ± 3 mV. The $–NH_3^+$-terminated particles (green line) have a mean ζ potential of +24 ± 6 mV. The PEG-terminated particles (blue line) have a mean ζ potential of 3 ± 2 mV.

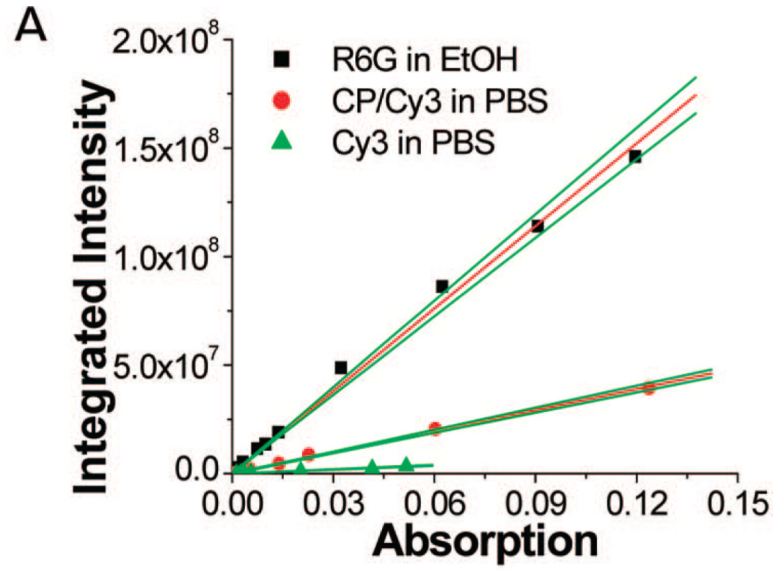

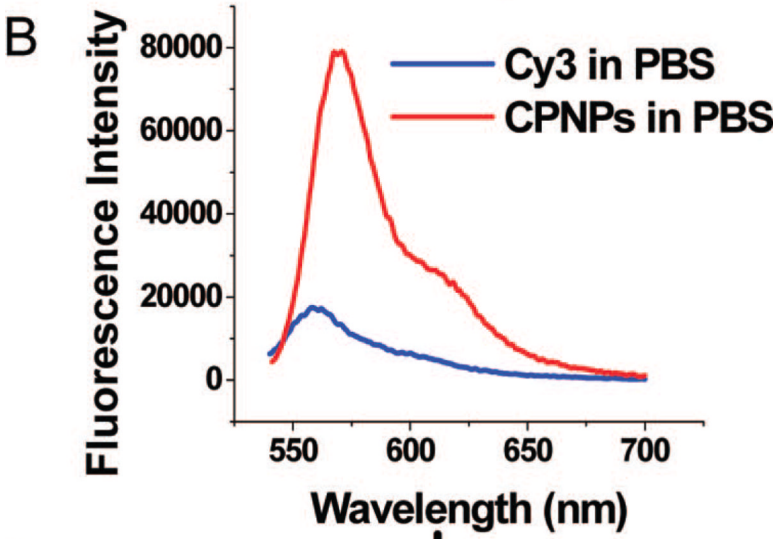

C

	QE
Cy3-CPNP	0.202+0.007
Cy3-Free Dye	0.045+0.002

Figure 6.

(A) The integrated fluorescence intensity versus the absorption at 532 nm for Cy3-CPNPs, Cy3-free dye, and rhodamine 6G as a reference. The slope of the line is used to calculated the quantum efficiency via eq 1. (B) Emission spectra of Cy3 encapsulated in calcium phosphate nanoparticles (CPNPs, red) and in free solution (blue) with an excitation of 532 nm. The solutions were tailored to have the same absorption at 532 nm. The maximum intensity of the CPNPs is more than 4.5 times the maximum intensity of the free fluorophore. (C) The quantum efficiency of the Cy3 encased in CPNPs (0.202), and the Cy3 in free solution (0.045).

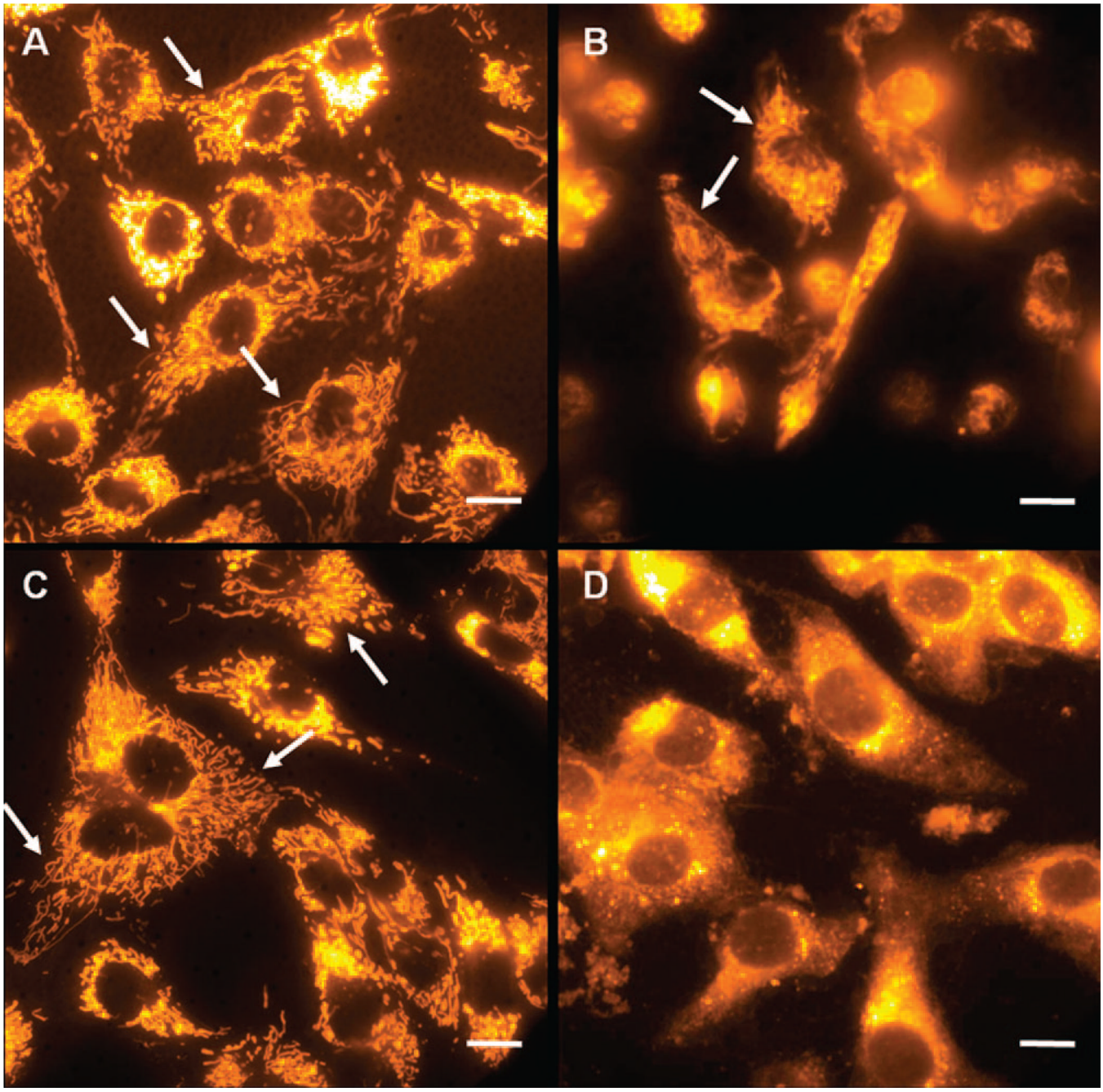

Figure 7.

Bovine aortic endothelial cells were stained with free Cy3 and were either untreated (A), or treated with cytochalasin-D (Cyto-D) (B) to inhibit fusion of endosomes to lysosomes during end-stage endosome formation. The staining patterns of the free dye were compared to the pattern of the cells that were stained with Cy3-encapsulated citrate-functionalized calcium phosphate nanoparticles (Cy3-CPNP) which were either untreated (C) or treated with cyto-D (D). The internal membranous organelles show specific staining in both of the untreated sets of cells (indicated by arrows in A and C). Cy3-stained cells treated with Cyto-D also show staining of organelles (C, indicated by arrows); Cy3-CPNPs do not stain the

internal membranes when the cells were treated with Cyto-D, indicating the particles remain undissolved (D). The scale bars are 10 μm.

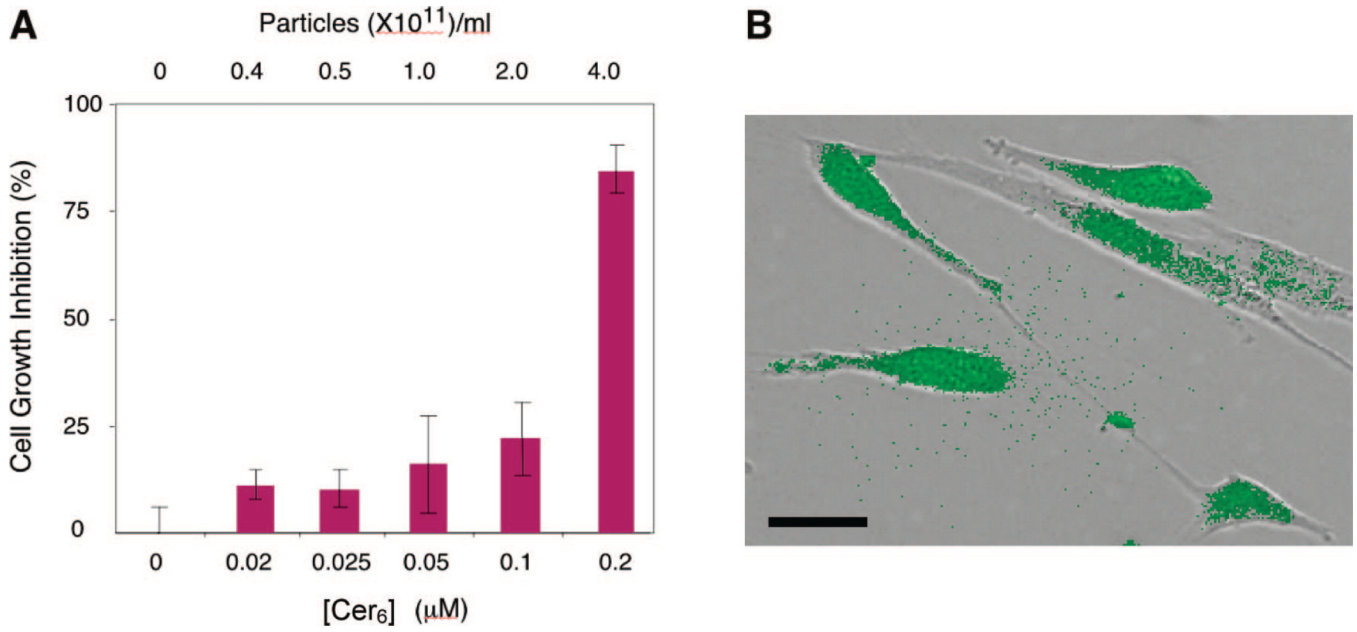

Figure 8.

(A) Growth inhibition of vascular smooth muscle cells as a function of concentration of Cer_6 delivered via CPNPs, and (B) image of the cells showing the fluorescence overlaid with the differential interference contrast image. The cells retain their morphology indicating no apoptotic or cytotoxic effects. The scale bar is 20 μm.